Sādhanā (2025) 50:218
https://doi.org/10.1007/s12046-025-02836-5

Enhancing the aerodynamic performance of a biomimetic wing with topography optimization

MEHMET E ÇALIŞKAN[1], MUHAMMET U SABIRLI[2], EMRE ORUC[2] and IRFAN KARAGOZ[2,3,*]

[1]Mechanical Engineering, Istanbul Health and Technology University, Istanbul, Turkey
[2]Mechanical Engineering Department, Engineering Faculty, Bursa Uludag University, 16059 Bursa, Turkey
[3]Ulutek Technopark, Bursa, Turkey
e-mail: mehmet.caliskan@istun.edu.tr; usamesabirli@uludag.edu.tr; emre.oruc16@gmail.com; karagoz@uludag.edu.tr

MS received 6 January 2025; revised 2 April 2025; accepted 9 April 2025

Abstract. This paper presents the optimization of the external shape of a model wing obtained from samara (maple seed) by means of biomimicry in order to improve its aerodynamic performance. Samaras, winged seeds of maples, have drawn attention in biomimetic design because of their high lift and low drag properties and autorotation capability. This makes them ideal for winged structures, which can operate in a wide range of wind conditions. This study aims to demonstrate that a samara wing can be modified using mathematical modelling, and different surface geometries can be created by making desired changes in the design parameters. Optimization of the topography of a samara wing model is presented using the results of computational fluid dynamics (CFD). The model wing was divided into three regions, and topography optimization was performed in five steps. Intermediate forms and final forms of the model are presented together with the CFD results. The final form of the model provided an aerodynamic performance increase of up to 28% depending on the angle of attack. In addition, as a result of these improvements, the biomimetic wing has simpler design parameters and a more applicable structure. These results suggest that aerodynamic performance can be enhanced by topography study on a biomimetic wing.

Keywords. Wing aerodynamics; renewable energy; bio-inspiration; aerodynamic performance; Leading Edge Vortex (LEV); turbines.

1. Introduction

Throughout history, humanity has always been influenced by its environment. Especially for architects

and designers, the different forms, techniques and functions of nature have been sources of inspiration [1, 2]. In the field of aviation, air vehicles with gliding or flapping wings, designed based on flying biological organisms, are being developed at an increasing pace [3–6]. These designs inspired by nature are called biomimetics, a term coined by Schmitt. Historically, the most famous biomimetic concept wing designs can be traced back to the dreams of Leonardo da Vinci [7]. With the advancement of technology, scientists' inspiration from nature and the processes of imitating nature have created a new scientific discipline [2]. Even design and optimization algorithms inspired by nature have been developed [8–10].

The concept of biomimicry is basically based on understanding and interpreting the physical basis of a process or adaptation found in nature, and then using these principles to provide new techniques to solve a new engineering problem [11–13]. One of these problems is the effect of flow separation, which is the subject of aerodynamics. Most designers focus on aerodynamic shape-oriented designs to reduce high drag forces. However, contrary to popular belief in some cases, nature shows the opposite. The dorsal structures of leatherback turtles (Dermochelys coriacea) exist in nature to create vortices along the flow and delay flow separation [14]. In another study, it was observed that the aerodynamic performance of steam turbines operating at low loads decreased significantly. One of the biggest reasons for this is flow separation effects. Wu *et al* [15] conducted an improvement study based on the fin of a humpback whale and analyzed the peak and trough effects. In this way, they observed that the impeller power of the bladed turbine with biomimetic design increased by 7.8% compared to the original design. Experiments in the wind tunnel showed that the ridges in front of the humpback whale fins developed as a model caused significant reductions in lift at high angles of attack. Van Nierop *et al* [16] investigated the effects of stall delay by increasing the amplitude of the ridges in the

*For correspondence
Published online: 29 August 2025

aerodynamically designed model. They found that the stall delay is insensitive to the wavelength of the ridges, in agreement with experimental observations.

Green Energy has gained significant value in line with increasing global demand. Biomimetic airfoils fill a large gap in this field. In a study by Montoya *et al* [17] a turbine blade was designed inspired by bird wings of the Guillemot (Uria aalge) species to improve turbine efficiency. Experimental tests were performed with reference to the Betz approach, and a higher lift-to-drag ratio was obtained at lower speeds.

Chu [18] designed a new biomimetic design of a marine current turbine inspired by the Dryobalanops aromatica seed. Since the two main factors determining the performance of marine current turbines are hydrodynamic performance and steering capability, the design is based on these two performance parameters. The studies were carried out using open source OPEN FOAM software using computational fluid dynamics (CFD) methods and the hydrodynamic performance and steering characteristics of the proposed biomimetic turbine were compared with some conventional turbines in the literature. The results show that the designed biomimetic marine current turbine provides optimum output power. It was also found that the designed biomimetic turbine produced significantly more torque under the same boundary conditions compared to conventional designs.

Samaras are one of the interesting examples used in biomimetic designs. In particular, the superior autorotation properties of samaras have made them popular in the fields of wind turbine design, renewable energy technology, and biomimicry [19]. In their experimental and numerical study, Lv *et al* [20] focused on a biomimetic technique that can be applied in a simple way to reduce the transonic emissions from conventional wind turbine blades. As a result, they found that the noise generated by the turbine blades significantly reduced both the infrasound and the overall sound pressure level.

In the study by Tangerman *et al* [21], the gliding capabilities of hovering birds were analyzed with reference to hovering birds. As a performance parameter, the minimum cruise speed of a white stork is considered. The wingtip of the white stork was designed in a computerized environment and tested using RANS and hybrid RANS-LES computational methods. As a result, the results are in good agreement with the literature. In this way, the analyses have helped to understand the basic flow physics at the wingtip of white storks and to analyze the aerodynamic effects at the wingtip point in more detail and to analyze the vortex effects.

One application area where bio-inspiration is being widely studied is wind turbines. The review article by Rtahod *et al* [9] presents bio-inspired designs of wind turbines, along with a detailed description of the relevant bio-organism and natural phenomenon, and classifies them for future designs. Li *et al* [22] presented a multi-rotor design with a biomimetic rotor configuration based on the optimal combination of blade configuration and pitch. In this way, they performed numerical simulations to determine the optimum aerodynamic performance. Although most studies in the literature focus on wing designs and their aerodynamic performance, the effect of rotor configurations still needs to be fully understood. A computational fluid dynamics (CFD)-based study was carried out for a four-rotor drone with a biomimetic design based on the criteria of propeller tip distance, height difference, and pitch angle. As a result, they observed that propeller tip distance and height difference play an important role in improving flight performance.

In another study, the production and experimental tests of a mini-sized wind turbine designed with an innovative approach were presented. Based on biomimetic methods, the design optimizes aerodynamic efficiency at low Reynolds numbers by using the shape and behavior of maple samara. The turbine dimensions are 44 mm in diameter and designed with the horizontal axis. The mini turbine tested at wind velocities between 1.2 and 8 m/s, has shown one of the highest performances in terms of efficiency and power density compared to other mini wind turbines in the literature. It also has a wide range of air speeds in terms of energy harvesting capability, with the lowest operating velocity of 1.2 m/s [23].

Ulrich *et al* [24] designed prototype geometries inspired by samara geometries and conducted a detailed experimental study showing the similarities between mechanical and robotic samara flight dynamics. Throughout the flight, they observed that the path of the helical orbits of the samara at the time of flight and the descent velocity varied. They emphasized that the angular ratios of body roll and pitch for different trajectories are linked to changes in wing pitch, thus providing a control method. After these experiments, inspired by the aerodynamic effects of biomimetic samaras, they developed a robotic device that models the autorotative property of the samara and offers the ability to translate, ascend, and hover. They used a high-speed camera-assisted motion capture system to evaluate the aerodynamic performance of the device. As a result, it is presented that the experimental system is suitable for this type of research and provides a platform for testing various wing efficiencies while studying wing structures.

Caliskan *et al* [25] determined the lift and drag force coefficients of the M0 biomimetic model experimentally and numerically at three different speeds and varying angles of attack. It is also noteworthy that the data in their experimental and numerical studies are in high agreement with each other for each combination.

In addition to experimental studies, mathematical modeling and optimization techniques are also used in the development of wing shapes or air vehicles [26, 27]. Topology optimization, which offers large design freedom and is used in a wide range of engineering fields, is also applied to wing structures. Gomes and Palacios 2020

proposed a two-step methodology to optimize external shape and internal topology of airfoils. In the first step, coupled fluid-structure interaction simulations are considered to minimize drag [28]. The second step is a stage that solves the inverse design problem and produces a discrete topology structure that responds identically to the fluid loads. In another study, Gomes and Palacios 2022 applied topology optimization to obtain a wing structure that allowed mass reduction without loss of lift. The conservation equations for turbulent flow were solved together with the structural strain equations to simulate the fluid-structure interaction [29]. A wing structure constructed from a combination of flexible and rigid material is proposed, ensuring that the outer layer is never left unsupported.

A study on the simultaneous optimization of the external shape and internal topology of wings to minimize drag is presented by Høghøj *et al* [30]. The aerodynamic and structural responses are modelled using the panel method and the linear elastic finite element model, respectively. A wing with NACA 2412 airfoil was used as a model. The optimization method was applied for cases with and without struts. For each case, only twist and both twist and chord length were considered to optimise the wing shape. Analysis showed that drag could ultimately be reduced by up to 32%.

In recent years, numerical optimization techniques have been widely used with the advances in computational techniques and computers [31]. A general methodology for delaying the dynamic stall of airfoils through aerodynamic shape optimization has been proposed by Raul and Leifsson [32]. The optimum airfoil shape was determined through the use of data from computational fluid dynamics simulations with the SST turbulence model. The results show that the optimum airfoil shape delays the dynamic stall angle by more than 3°. On the other hand, Abolpour *et al* [33] have proposed a new approach to achieving minimum drag through optimum shape design. They developed a genetic algorithm combined with image processing for shape optimization. The drag coefficient was obtained by solving the conservation equations for the turbulent flow around the obstacle at each improvement step. Verification was carried out by comparing the computational results with the experimental results.

In this study, a method for optimization of a biomimetic wing is presented and applied for the first time. Based on a wing model inspired by maple seed in the previous studies [25], the proposed topographic optimization method is applied in five steps and the improvement in aerodynamic performance is examined at each stage. The results show that significant improvement in aerodynamic performance is achieved.

2. Numerical and experimental studies

A wing model (M0) inspired by maple seeds is considered as the basic wing in this study. The aerodynamic performance of this model was improved through a 5-stage optimisation study. At each stage of the optimisation study, the results of CFD analyses performed on the improved model were used.

2.1 *Numerical methods*

Conservation equations of three-dimensional turbulent flow were used in the flow modelling and these equations were solved using Fluent software. Considering the performance of the studies, the Shear Stress Transport (SST) k-ω model, which is a turbulence model with higher compatibility with experimental data in confined flow, was selected as the turbulence model to be used in this study.

The test section of the wind tunnel used in the experimental study was modelled in the design software. In order to perform the numerical analysis under the boundary conditions of the experimental model, the wing model was appropriately placed within this flow domain. These boundary conditions are shown in the flow field in figure 1. The geometry containing this flow field was designed individually for each angle of attack and transferred to Ansys for numerical analysis.

The volume around the wing, which can be seen in figure 1, aims to create finer meshes around the wing in the flow field. In this flow field, where the tetra mesh structure is used, the infiltration from the wing surface is also defined. In this mesh structure, shown in figure 2; a section taken from the A-A line (a) shows the general structure of the meshes within the flow field (b) and the finer meshes around the wing (c).

In this numerical study, the SIMPLE scheme was chosen for the calculation of the steady state pressure fields with the Second Order Upwind in order to obtain a high accuracy. Since experimental data were also used to verify the converged numerical results, a three-dimensional solution

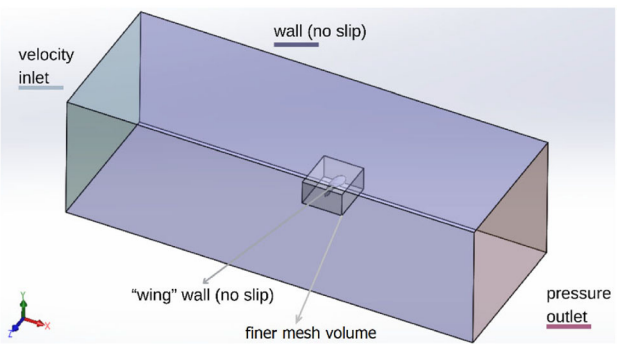

Figure 1. Boundary conditions in the computational domain

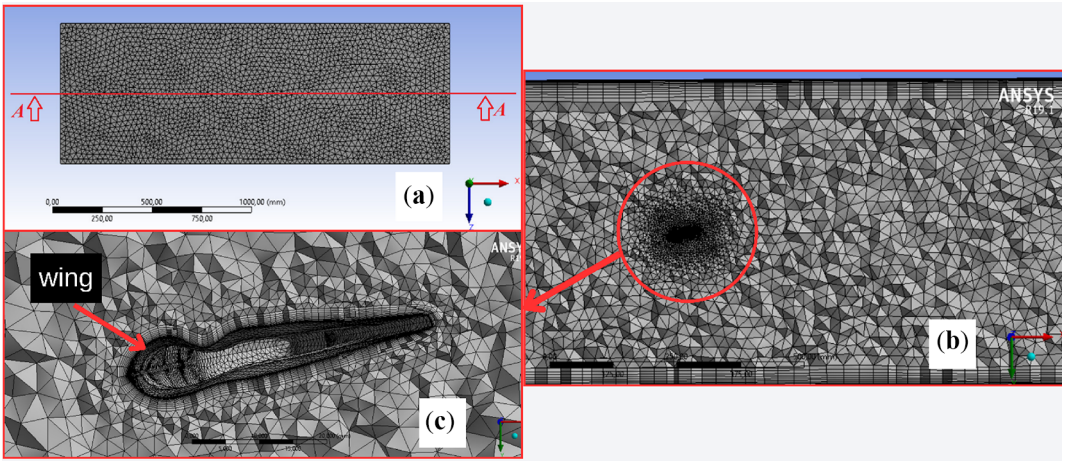

Figure 2. General (a), cross-sectional (b) and wing model zoomed-in (c) view of the generated mesh structure

field model suitable for the experimental system was created for the CFD analysis. A tetrahedral mesh structure was used to best represent the shape of the model in the flow field. The mesh structure near the wing model becomes denser towards the model in order to make the model compatible with the surface topography.

The mesh independence study was carried out using coarse, medium, fine and very fine mesh structures with mesh element numbers of 850k, 1450k, 2400k and 5000k respectively. When examining the changes in the performance parameters, lift coefficient (C_L) and drag coefficient (C_D), it was found that the change was at a negligible level for mesh numbers greater than the medium mesh size, so numerical analyses were carried out using 1450k meshes.

The average skewness parameter for the mesh used is 0.22 and the maximum skewness is less than 0.8. In addition, the grid convergence index (GCI) and the asymptotic value were calculated for this grid as 0.16% and around 1, respectively, which also shows that convergence occurs asymptotically. In addition, to validate the numerical results, the aerodynamic performance of the generated wing models was measured experimentally for certain cases and compared with the numerical results.

2.2 *Experimental methods*

Experimental studies were carried out in an open-loop wind tunnel. This low-speed tunnel is a suction type wind tunnel with a 4 kW fan and a test area of 40×40×100 cm. The turbulence intensity of the tunnel is less than 1% and the contraction ratio is 9:1. A schematic view of the test and measurement system is shown in figure 3.

In the wind tunnel, the speed of the air in the test section, and therefore its dynamic pressure, can be changed with a frequency-controlled fan. To determine the aerodynamic performance of the wing, a 6-component ATI Gamma model transducer system with load cells was used. The force measurement range in the system is up to 100 N and the resolution is 1/160 N.

The free flow velocity in the tunnel was measured using a Mano Air 500 micromanometer in the test section of the tunnel. The temperature and humidity probe of this micromanometer, which obtains 2 readings per second with an accuracy of ±0.5 Pa, can also measure the temperature values (T_∞) of the fluid.

An error analysis was also carried out on the experiments and the experimental results obtained for the lift and drag

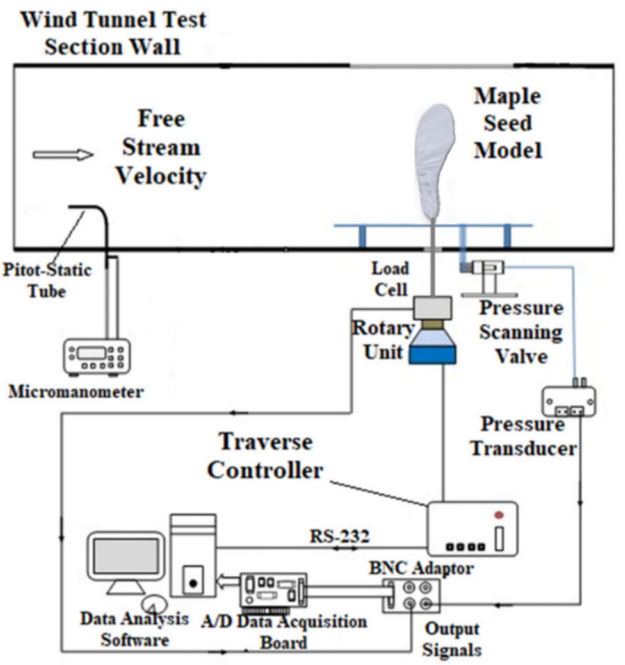

Figure 3. Schematic representation of the experimental system

coefficients. The lift and drag coefficients used as aerodynamic performance criteria are calculated as follows:

$$C_L = \frac{L}{0{,}5\rho {V_\infty}^2 S} \tag{1}$$

$$C_D = \frac{D}{0{,}5\rho {V_\infty}^2 S} \tag{2}$$

where; L and D are the lift and drag forces obtained from the force measurements, respectively, V_∞ is the free flow velocity, ρ is the air density, S is the planform area of the wing model. Therefore, the total errors of the C_L and C_D values are;

$$\begin{aligned}\Delta C_L &= \sqrt{\left(\frac{\partial C_L}{\partial L}\Delta L\right)^2 + \left(\frac{\partial C_L}{\partial S}\Delta S\right)^2 + \left(\frac{\partial C_L}{\partial V_\infty}\Delta V_\infty\right)^2} \\ &= \sqrt{\left(\frac{1}{0{,}5\rho {V_\infty}^2 S}\Delta L\right)^2 + \left(\frac{-L}{0{,}5\rho {V_\infty}^2 S^2}\Delta S\right)^2 + \left(\frac{-2L}{0{,}5\rho {V_\infty}^3 S}\Delta V_\infty\right)^2}\end{aligned} \tag{3}$$

$$\begin{aligned}\Delta C_D &= \sqrt{\left(\frac{\partial C_D}{\partial L}\Delta L\right)^2 + \left(\frac{\partial C_D}{\partial S}\Delta S\right)^2 + \left(\frac{\partial C_D}{\partial V_\infty}\Delta V_\infty\right)^2} \\ &= \sqrt{\left(\frac{1}{0{,}5\rho {V_\infty}^2 S}\Delta D\right)^2 + \left(\frac{-D}{0{,}5\rho {V_\infty}^2 S^2}\Delta S\right)^2 + \left(\frac{-2D}{0{,}5\rho {V_\infty}^3 S}\Delta V_\infty\right)^2}\end{aligned} \tag{4}$$

For ΔS, 0.05 mm, which is the maximum error of the 3D printer from which the wing model was produced, was taken as the square of 0.025 mm due to the area calculation. For ΔL and ΔD, which are the errors of the lift and drag forces, the standard deviations of the obtained force measurement data were used. To calculate ΔV_∞, the dynamic pressure error ΔP_{dyn} must first be known. The dynamic pressure error ΔP_{dyn} was taken as 2 Pa from the instrument catalogue and the velocity error; $\Delta V_\infty = \frac{\Delta P_{dyn}}{\rho\sqrt{\frac{2P_{dyn}}{\rho}}}$ was calculated for each velocity value with the P_{dyn} value measured by the instrument. As a result of these calculations, the error for the lift and drag coefficients was found to be less than 8%, which is acceptable. In addition, the error bars for the lift and drag coefficients for one case are shown in figures 18 and 19. Further details on numerical and experimental methods can be found in [25].

3. Topography optimization

Topography optimization is changing the structures, such as indentations, that make up the shape of an object in a way that improves its desired performance. In the present topography optimization, the previously designed wing model inspired by maple samara [25] was taken as basis model and named as the model M0.

The model wing designed in the computer environment was divided into a certain number of sections and each section shape was defined by curves expressed by Fourier series equations. After determining the curves, the shape of the M0 model will be optimized in five steps, keeping the planform area ($\boldsymbol{b}(\boldsymbol{spanlength})\times\boldsymbol{c}(\boldsymbol{meanchordlength})$) constant. In figure 4, the curves that make up the skeletal structure in different cross-sections of the model with labels can be seen. These labels are symbolized by "S" for the seed part, "T" for the transition part and "L" for the leaf part of the biomimetic model, and numbered in order.

Each of the curves forming the surface is described by a general Fourier series equation. The terms of the series are taken as many as are needed to describe the curve and in this way the mathematical expression of the curves is formed. The general structure of the n-term finite trigonometric series containing the sin and cos terms is given in Eq. 5.

$$\boldsymbol{y} = \boldsymbol{a}_0 + \sum_{i=1}^{n} \boldsymbol{a}_i \mathbf{cos}(\boldsymbol{ixw}) + \sum_{i=1}^{n} \boldsymbol{b}_i \mathbf{sin}(\mathbf{ixw}) \tag{5}$$

The curves of the M0 biomimetic model generated by the mentioned equation and all design details can be found in the previous study [25].

In this study, a topography optimization is performed using some numerical results, the details of which can be found in the same basic study. Caliskan *et al* (2023), carried out numerical and experimental investigations for the M0 wing model up to 45 degrees angle of attack at variable free stream velocities and presented the results with numerical flow visualisations and data [25]. The data and numerical visualisations of the M0 model used in the first stage of the topography optimization study were also obtained from this study. The operating conditions chosen for this topography

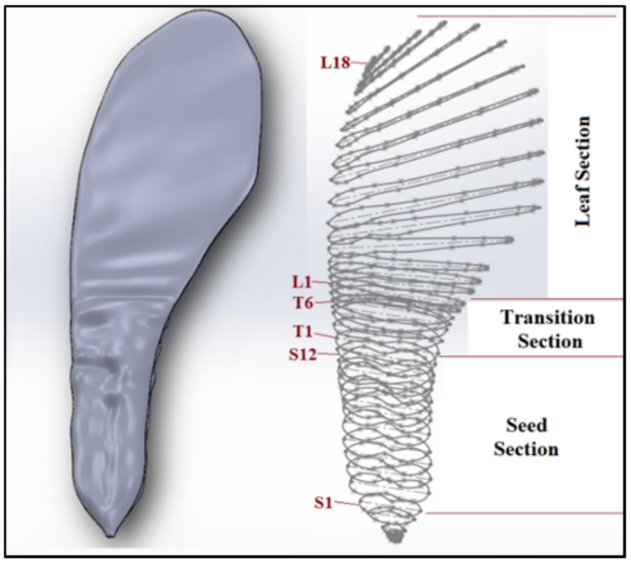

Figure 4. Curves forming the skeletal structure of the M0 model

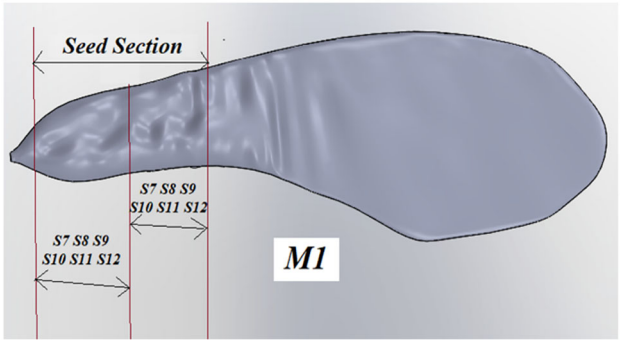

Figure 6. M1 model

study are a free stream velocity V_∞:10 m/s and one of the best performing angles of attack α: 10°. The development study will be interpreted according to the numerical data obtained in this configuration.

Lift force is an important aerodynamic parameter especially in conventional vehicles where wings are used. Considering that the main phenomenon that creates the lift force in the wings is the pressure difference occurring on the upper and lower surfaces, the increase in this pressure difference will allow the lift force of the wing to increase. Caliskan *et al* [25], mentions that the structure that creates the pressure difference of M0, the biomimetic wing model they created, is the Leading Edge Vortex phenomenon, which is also mentioned in case studies where many biological wing structures are examined [34–39].

In the M0 model, the area where the lift force affects the wing surface the most is in the seed section, as can be seen in figure 5, and the equations representing this area are the 6 curves seen in the figure with the labels S7, S8, S9, S10, S11 and S12.

As can be seen from this figure, the curves in the second half of the seed that create the highest pressure difference; S7, S8, S9, S10, S11, S12 curves were substituted for the S1, S2, S3, S4, S5, S6 curves in the other half of the seed, respectively, and the "M1" model in figure 6 was obtained. These curve changes on the wing structure are made on a design programme in such a way that the planform area of

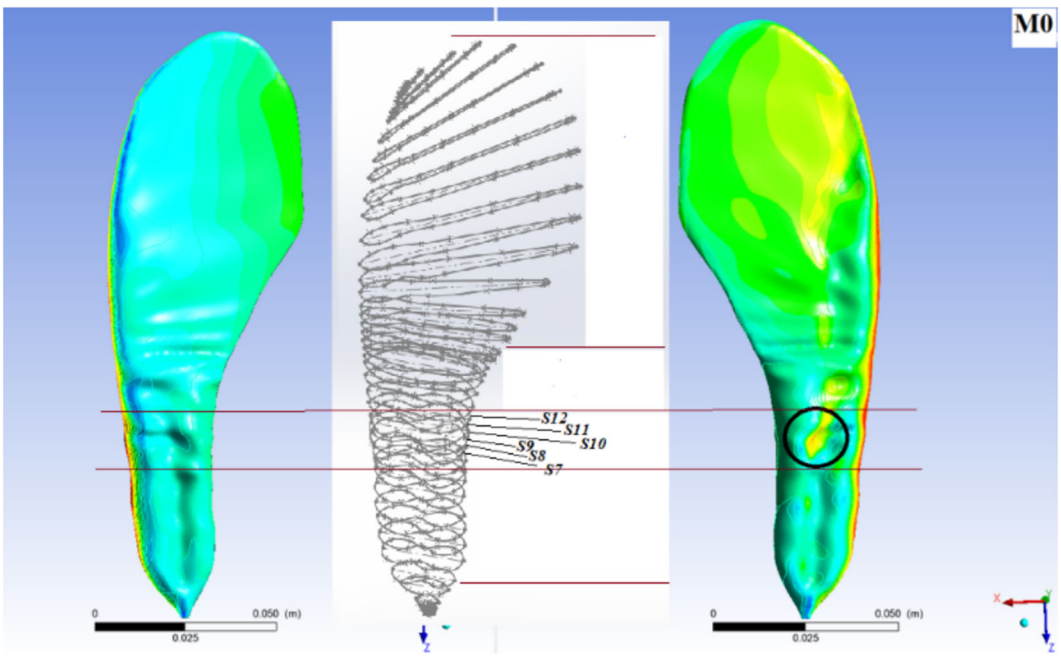

Figure 5. Pressure contours of model M0 for α:10°, V_∞:10 m/s and 6 curves forming the highest pressure difference

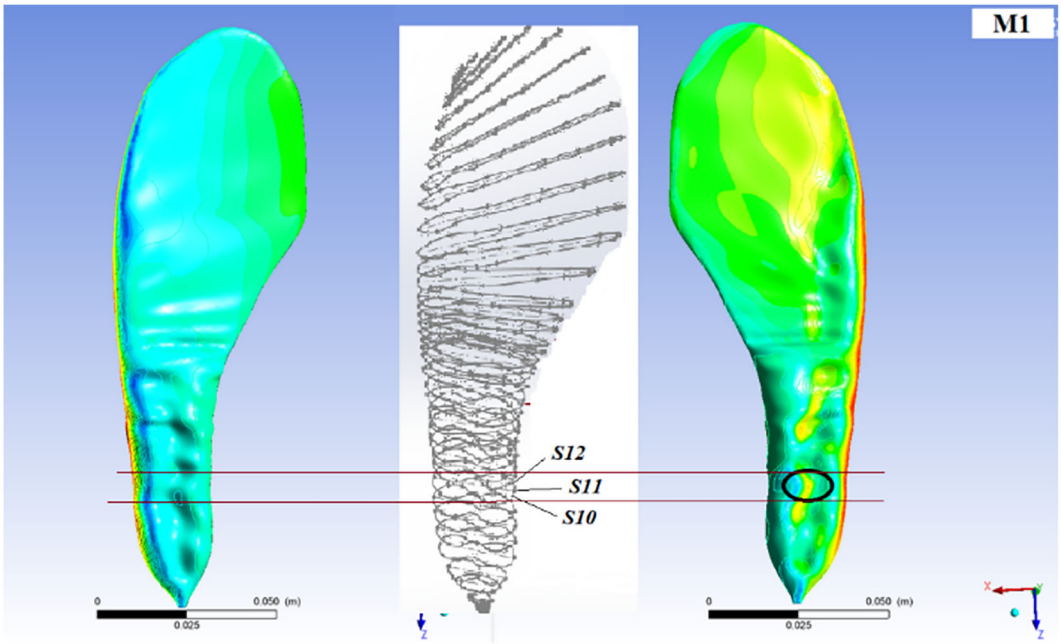

Figure 7. Pressure contours of model M1 for α:10°, V_∞:10 m/s and 3 curves forming the highest pressure difference

the wing does not change thanks to the design details of the M0 model given. Method of change on design aims to expand the surface properties that make up the high pressure difference to the entire seed. Therefore, the higher lift force caused by the higher pressure difference will provide an enhancement in the aerodynamic performance of the wing. With the development of the M1 model, the first stage of the topography optimization study consisting of 5 stages was completed.

For the model M1, just as in the M0 model, numerical analysis was performed at α:10° and V_∞:10 m/s. As a result of this analysis, the pressure contours in figure 7 were obtained. The numerical analysis modelling to be used in this and the subsequent wing models was similar to the numerical analyses applied by Caliskan *et al* (2023) [25] for the M0 model.

In figure 7, similar contour distributions formed in the two halves of the seed part of the M1 model show that the adaptation of half of the seed to the other half was successful. Like this, it has also been seen that similar pressure differences can be achieved on the surface by imitating the topographical feature. Similar to the previous step, the small part shown in the circle, where a higher pressure difference occurs compared to its surroundings, is the area between the lines: S10, S11, S12 curves. With a similar logic, when these 3 curves are integrated respectively instead of 12 curves in the seed part, the "M2" model in figure 8 is formed. Thus, in the M2 model, the seed part is defined by 3 curves.

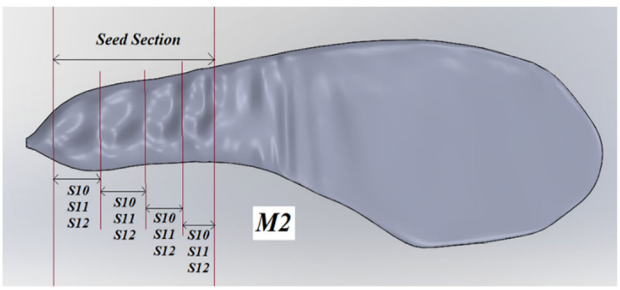

Figure 8. M2 model

After the numerical analysis for the M2 model under the same conditions (α:10° ve V_∞:10 m/s), the pressure contours obtained on the lower and upper surfaces of the model are given in figure 9.

Figure 9 shows that the pressure difference areas increase after the curve integration applied in the previous model. If the area where the highest pressure difference occurs is narrowed once again, the area represented by the curves S11 and S12 in figure 9 is obtained. The "M3" model in figure 10 was obtained by integrating these S11 and S12 curves, respectively, into the 12 curves in the seed part of the M2 model. The seed part of this model can be represented by 2 curves.

After the numerical analysis for α:10° and V_∞:10 m/s with the M3 model, the pressure contours obtained on the lower and upper surfaces of the model are given in figure 11.

With the M3 model, the curve adaptation and integration process in the seed part is also finished. Since the dimple structures forming the pressure differences are formed by arranging at least two curves one after the other, and the curves S11 and S12 are the curves that create the highest pressure difference, the number of curves cannot be further

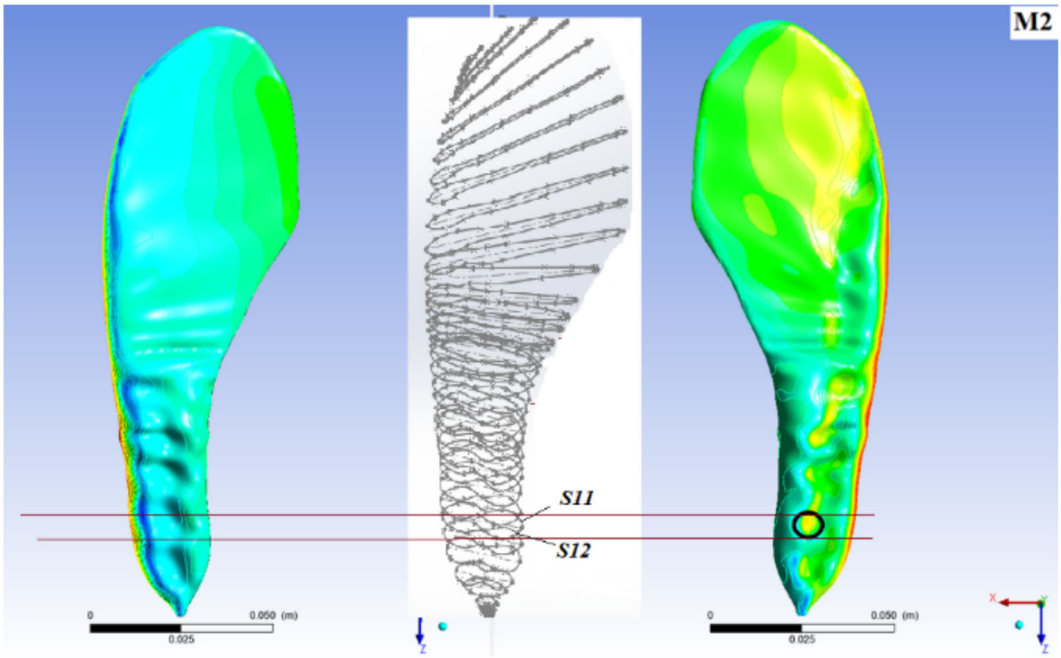

Figure 9. Pressure contours of model M2 for α:10°, V_∞:10 m/s and 2 curves forming the highest pressure difference

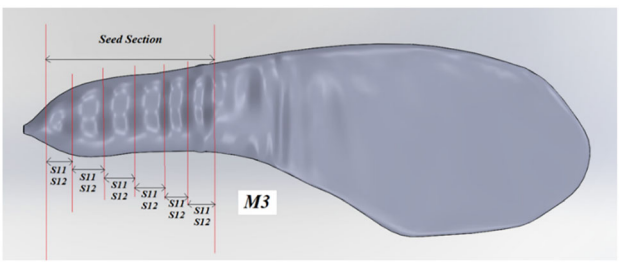

Figure 10. Model M3

reduced. After that, curve fitting studies will be carried out in other parts (transition and leaf parts) of the maple seed model.

Since the topographic optimization in the seed part was terminated with the M3 model, it was again desired to achieve both the highest aerodynamic performance and the least equation expression objectives with the changes in the transition and leaf parts of the model. For this, the S11 and S12 curve pair, which successfully showed its effect in the M1, M2 and M3 models, were integrated into the 6 curves in the transition part of the model, respectively, and the "M4" model given in figure 12 was revealed. In this model, the seed and transition parts can be defined with 2 curve equations.

After the numerical analysis for α:10° and V_∞:10 m/s with the M4 model, the pressure contours obtained on the lower and upper surfaces of the model are given in figure 13.

As can be seen from figure 13, it can be said that the desired pressure difference increase attempt in the first 4 stages of the optimization study was successful, with the warm colours spreading significantly on the upper surface of the wing. The development and optimization studies carried out up to this point have shown that the application of the curve pairs that create the high pressure difference on our biomimetic wing model to other areas can yield successful results. It is understood from the pressure contours given for the 4 models that the given curves increase the peak-dimple structures on the model and this causes an increase in the pressure differences.

With the M4 model, the seed and transition part can now be defined with 2 curves instead of 18 curves. However, the leaf part of the M4 still has 18 curves. As can be seen from the curve shapes, while the curves in the seed and transition parts are similar to each other, the curves in the leaf part are much thinner and sharper. Therefore, it is not desired to use S11 and S12 curves, the effects of which have been proven before, for the development process to be performed on the leaf part. Instead, the topographical effect of these two curves on the model surface was examined. This topographic effect is a peak-dimple structure, as seen in M1, M2, M3, and most clearly M4. For the leaf part, this structure formation was seen in several places on the geometry. However, the curves that would give the clearest peak-dimple topography were between the L7 and L8 leaf curves, as shown in figure 14. The highest peak-dimple structure in the leaf part is formed by the arrangement of these two curves.

The L7 and L8 curves, which are expected to give higher pressure differences when arranged in the whole leaf part, were integrated respectively instead of the 18 curves in the leaf part of the M4 model, and the "M5" model given in figure 15 was formed.

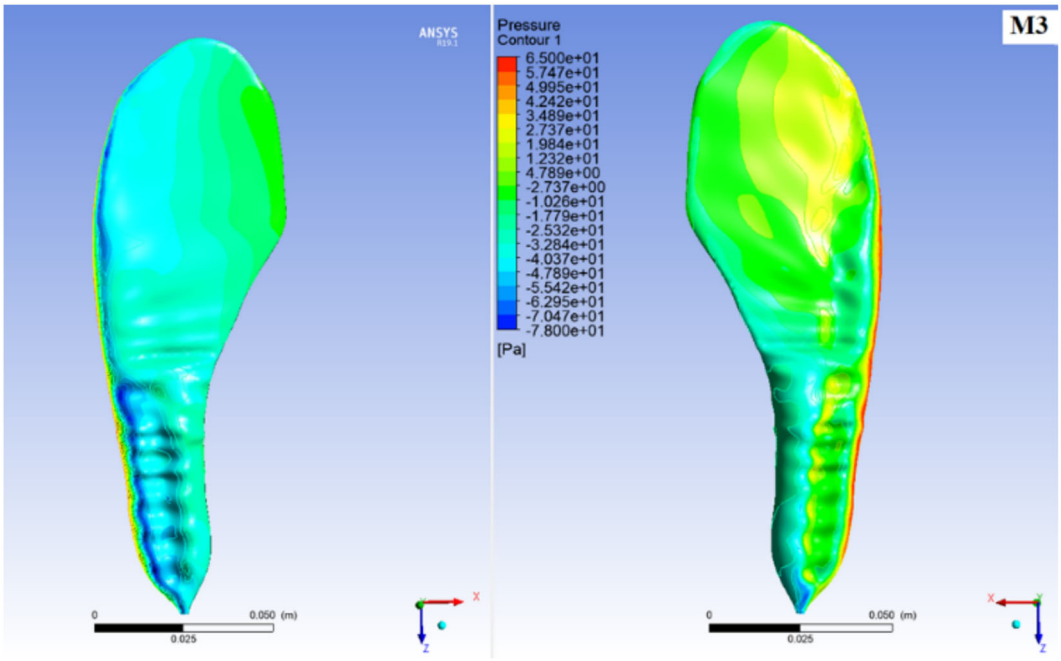

Figure 11. Pressure contours of model M3 for α:10°, V_∞:10 m/s

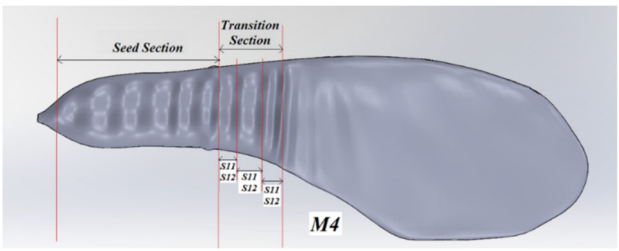

Figure 12. Model M4

After the numerical analysis for α:10° and V_∞:10 m/s with the M5 model, the pressure contours obtained on the lower and upper surfaces of the model are given in figure 16.

With the development of the M5 model, which can be defined with only 4 curves, the topography optimization was completed. As can be seen from figure 16; the pressure differences in the final model M5 are higher than M0.

4. Results

The pressure contours obtained from the numerical analysis of 5 models developed through topography study at a certain free stream velocity and angle of attack are given and the differences between them are pointed out. Since these contours are taken in the same pressure range and scale, the increasing yellow and red areas in the model developments towards the M5 model show us that the study increases the pressure differences on the lower and upper surfaces of the model. These pressure differences increase the lift coefficient and therefore the aerodynamic performance of the wing. In order to see this increase more clearly, in table 1, aerodynamic performance parameters and statistical development rates of the other 5 models created according to the M0 model are given. These parameters mentioned in the table are lift force coefficient (C_L) and drag force coefficient (C_D) which are dimensionless expressions.

As it can be seen in table 1, while the topography study carried out resulted in a generally continuous increase in C_L and C_L/C_D, there was almost no increase in C_D and even a lower C_D was obtained in the M5 model compared to the M0. In conclusion, looking at the aerodynamic performances, a C_L increase of 25.7% and a C_L/C_D increase of 28.1% were obtained in the M5 model compared to the M0.

Although M0 and M5 models show the same characteristics in terms of aerodynamic performance, the increase in the lift force provided by the M5 model is seen in the numerical results with the conditions in the M0 model in figure 17.

While the lift force coefficient is higher in the M5 model compared to the M0 model, it is observed that the drag force coefficient does not show a significant change. The drag force is the sum of the drag due to pressure (C_{Dp}) and friction (C_{Df}). Asadzadeh *et al* [40] showed that the creation of grooves on the surface usually leads to the creation of secondary vortices inside the grooves, which in turn affect the frictional and pressure drag. Figure 18 shows the drag force values due to pressure and friction for the two models.

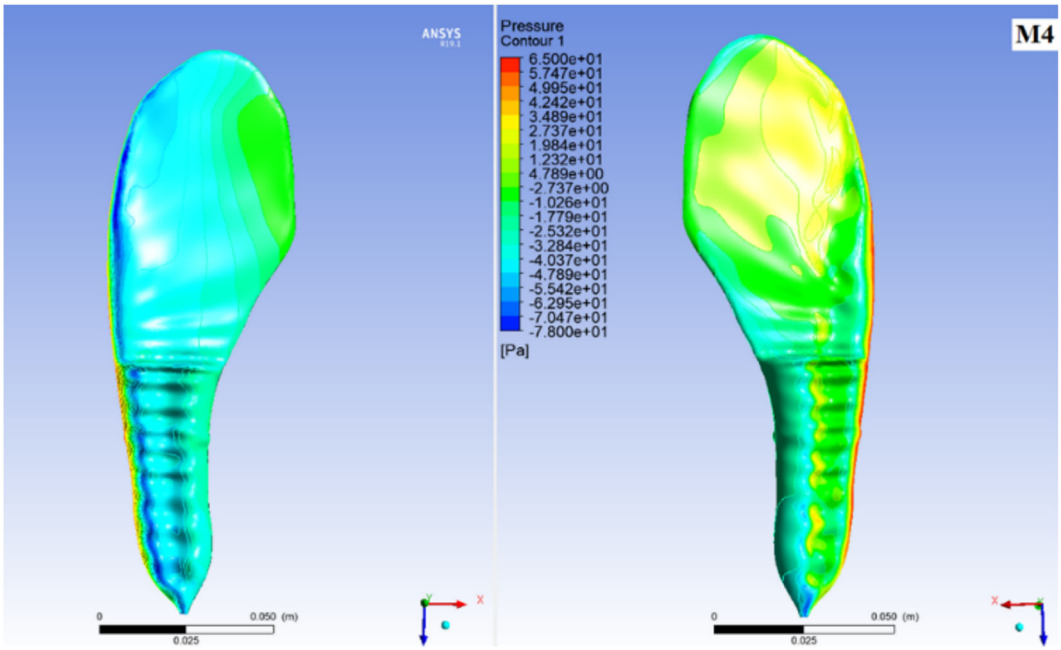

Figure 13. Pressure contours of model M4 for α:10°, V_{∞}:10 m/s

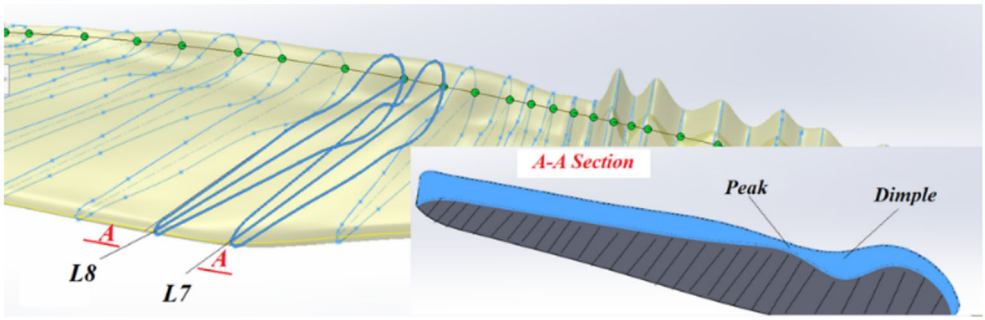

Figure 14. The peak-dimple structure formed by the L7 and L8 curves

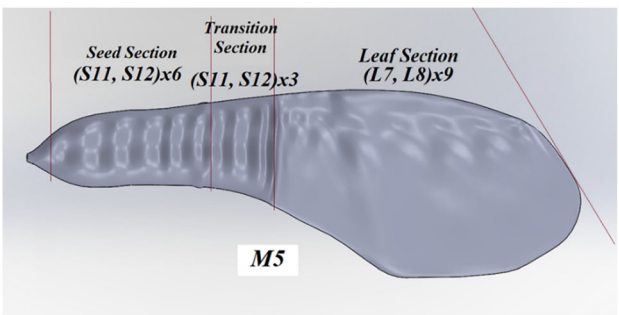

Figure 15. Model M5

The effect of the topography study on the drag force is seen only in the friction (viscous) drag. Here, it can be mentioned that there is a minor decrease in the drag force due to friction.

The purpose of topography optimization, in addition to increasing the aerodynamic performance of the biomimetic wing model, it also minimizes the curves that represent the model, and therefore, the equations. At the beginning of the optimization, in the model M0, the model was defined by 36 curves. In the model M5 obtained at the end of the study, this number was reduced to 4. We can see this change in detail in each model from table 2.

The quantitative and qualitative findings obtained from the topography study showed that the aerodynamic performance of the developed model M5 is worth examining. Therefore, the experimental and numerical methods of the M0 model were also performed for the M5 model. Therefore, the experimental study was carried out in the wind

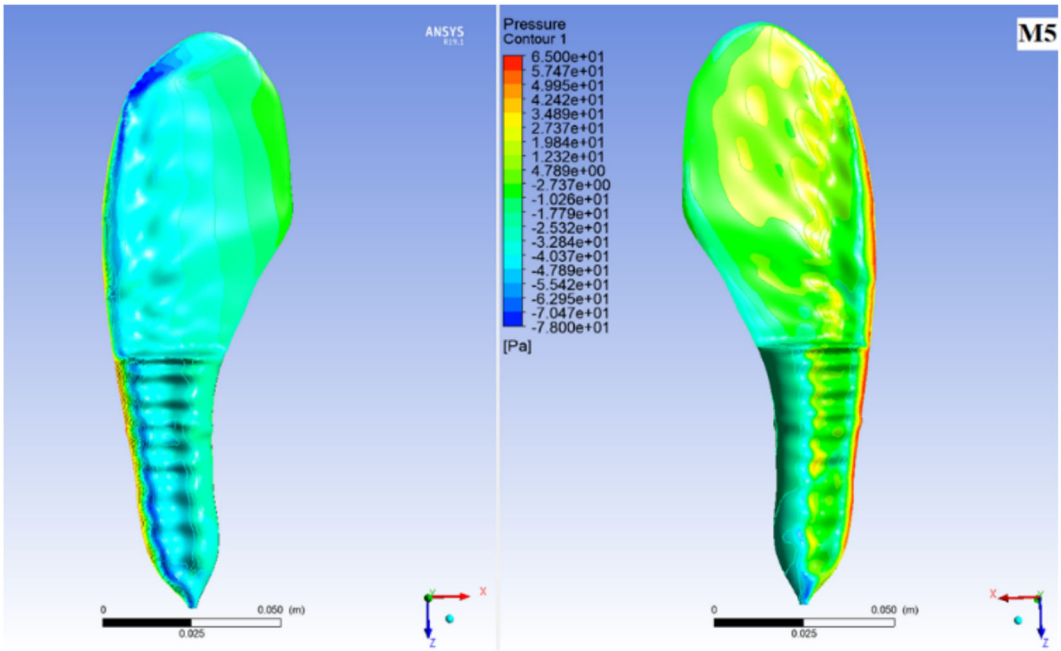

Figure 16. Pressure contours of model M5 for α:10°, V_∞:10 m/s

Table 1. Comparison of models obtained from topography optimization, aerodynamic performance at α:10° and V_∞:10 m/s and compared to M0

Topography Optimization				Compared to M0	
Model	C_L	C_D	C_L/C_D	Increasing rate of C_L	Increasing rate of C_L/C_D
M0	0,342	0,198	1,727	0%	0%
M1	0,375	0,202	1,856	9,6%	7,5%
M2	0,382	0,199	1,917	11,7%	10,9%
M3	0,394	0,192	2,05	15,3%	18,7%
M4	0,409	0,203	2,02	19,5%	16,9%
M5	0,430	0,194	2,213	25,7%	28,1%

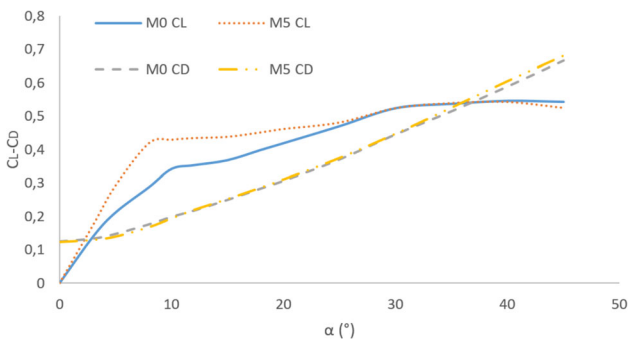

Figure 17. C_L and C_D variation of the M0 and M5 with respect to α at $10\boldsymbol{m/s}$ free stream velocity

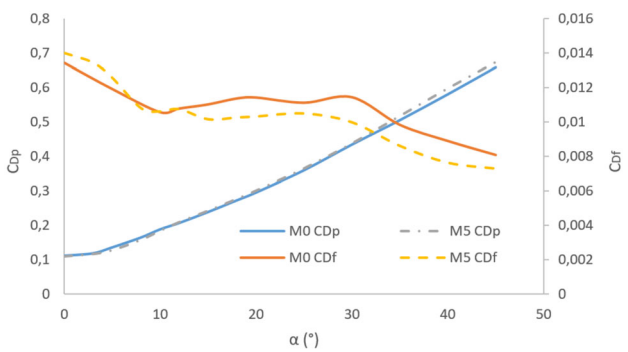

Figure 18. C_{Dp} and C_{Df} variation of the models with respect to α at $10\boldsymbol{m/s}$ free stream velocity

Table 2. Curves describing models from topography optimization

Model-Sections	Seed	Transition	Leaf	Total
M0	12 curves	6 curves	18 curves	36 curves
	S1…S12	T1…T6	L1…L18	S1…L18
M1	6 curves	6 curves	18 curves	30 curves
	2×(S7…S12)	T1…T6	L1…L18	S7…L18
M2	3 curves	6 curves	18 curves	27 curves
	4×(S10…S12)	T1…T6	L1…L18	S10…L18
M3	2 curves	6 curves	18 curves	26 curves
	6×(S11-S12)	T1…T6	L1…L18	S11…L18
M4	2 curves		18 curves	20 curves
	6×(S11-S12)	3×(S11-S12)	L1…L18	S11…L18
M5	2 curves		2 curves	4 curves
	6×(S11-S12)	3×(S11-S12)	9×(L7-L8)	S11-S12-L7-L8

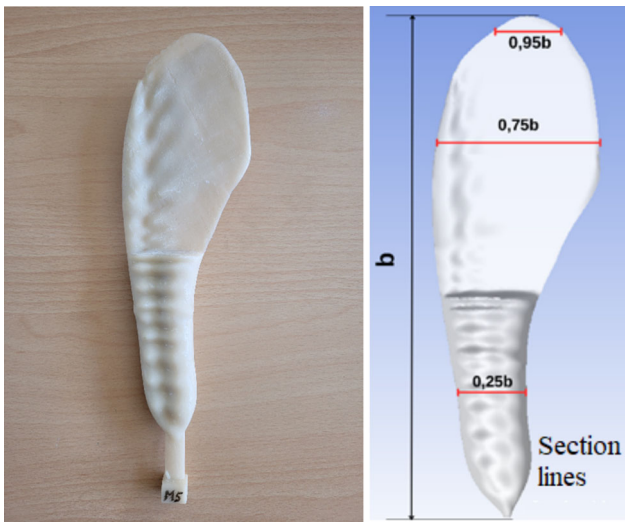

Figure 19. 3D printing of the model M5 for experimental work and section lines

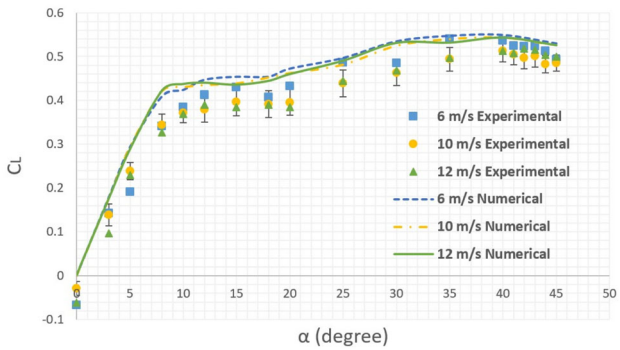

Figure 20. C_L variation of the model M5 with respect to α at different free stream velocities

tunnel in the aerodynamic laboratory of Niğde Ömer Halisdemir University.

The model M5 was produced with a 3D printer, in order to carry out its experimental work. The dimensions of this produced model, shown in figure 19, have the same dimensions as (span length b: 0.25 m, mean chord length c:0.0535645 m) of the M0 model.

The change in the lift coefficient of the model M5 at each free stream velocity for the positive angles of attack is given in figure 20, the variation of the drag force coefficient is given in figure 21, and the ratio of these two is given in figure 22.

These graphs show that the numerical and experimental results are in good agreement, and the aerodynamic parameters are very close to each other despite the varying free stream velocities. It was determined that the stall angle of the model M5 was around 44°, like the model M0.

For a better clarification of the focus of the topography optimization, the flow streamlines and pressure contours for M0 and M5 models are shown in figures 23, 24, 25, 26, which are cross-sections of the wings at certain distances (see figure 19) from the span dimensions.

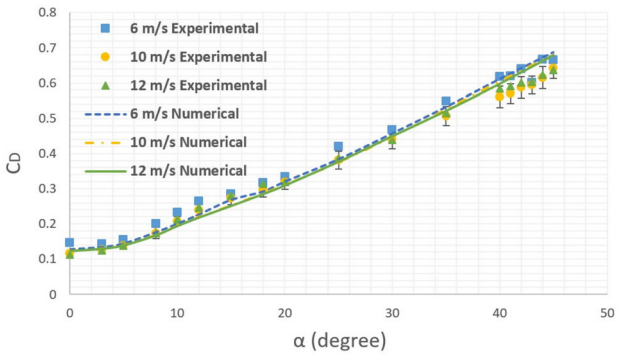

Figure 21. C_D variation of the model M5 with respect to α at different free stream velocities

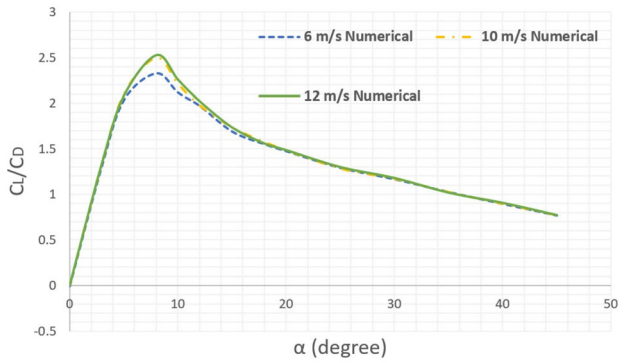

Figure 22. C_L/C_D variation of the model M5 with respect to α at different free stream velocities

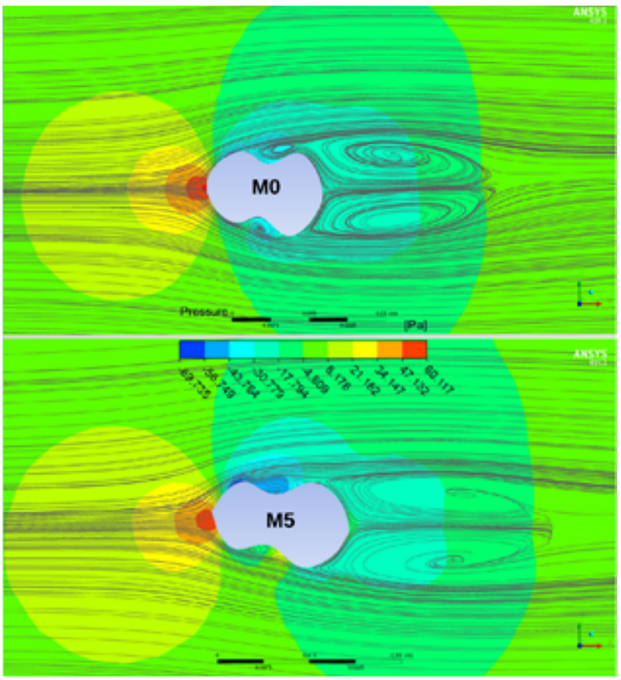

Figure 23. Pressure contours and streamlines at certain section (0.25b) of the M0 and M5 model for α:8° and V_∞:10 m/s

Especially when looking at the streamlines shown with red circles in figures 24 and 25, it can be seen that the Leading Edge Vortex (LEV) structure providing lift force to maple seed mentioned by Lentink *et al* [41], which provides the lift formation of the M0 model in the previous study (25), has developed and grown. This vortex structure, which grew with the effect of the topography study, created a stronger suction on the wing. This effect can be clearly seen in the vortex regions in the pressure contours given in the same scale for both wings.

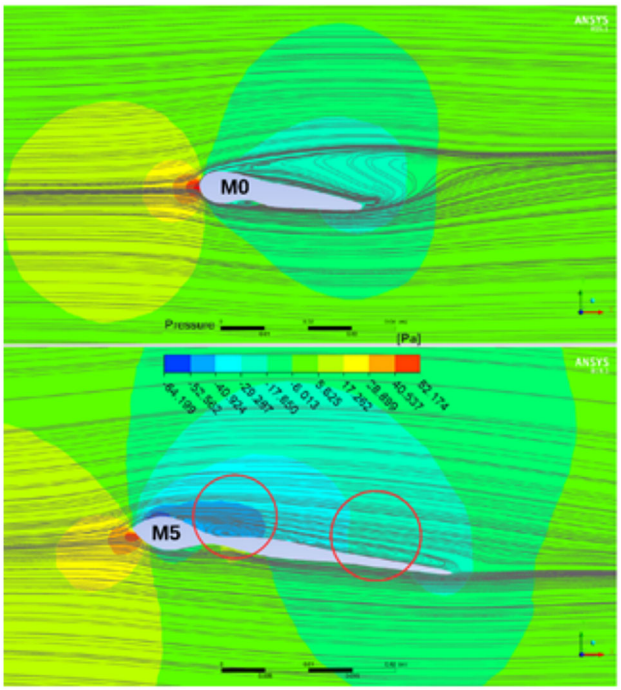

Figure 24. Pressure contours and streamlines at certain section (0.5b) of the M0 and M5 model for α:8° and V_∞:10 m/s

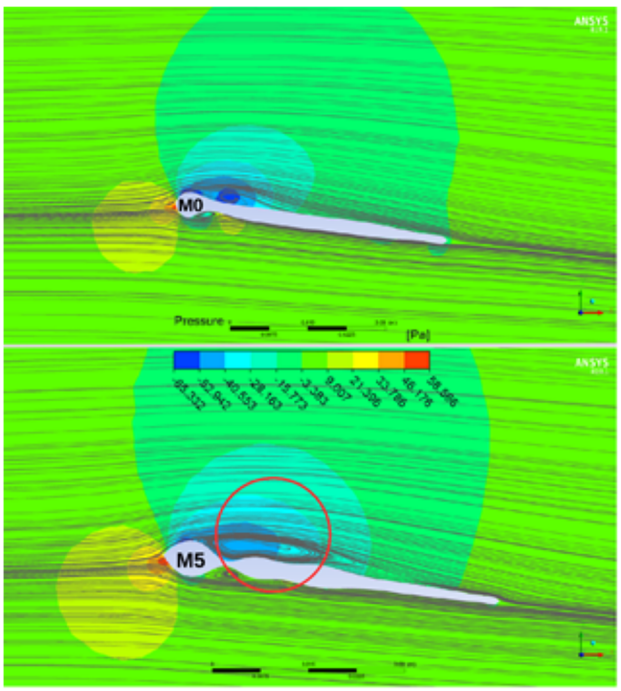

Figure 25. Pressure contours and streamlines at certain section (0.75b) of the M0 and M5 model for α:8° and V_∞:10 m/s

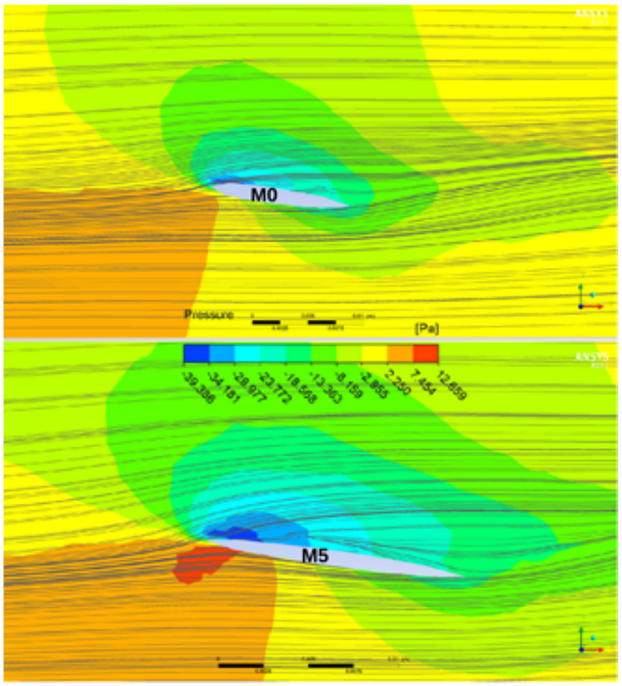

Figure 26. Pressure contours and streamlines at certain section (0.95b) of the M0 and M5 model for α:8° and V_∞:10 m/s

5. Conclusions

In this study, it is shown that a topography optimization can be performed to enhance the aerodynamic performance of a wing based on the different pressure areas formed on the wing. For this topography optimization, regions with high pressure differences determined on the surface topography of the model M0 had a positive effect. The model M5, created by spreading these regions into the general model structure, provided a performance increase up to %28 compared to the model M0, depending on the angle of attack. In addition, while the model M0 was defined with 36 equations, the M5 model could be defined with only 4 equations. This provided a more feasible solution for defining the design parameters of biomimetic wings with complex geometries.

In general, no LEV structures were seen in the lower part of the biomimetic wings. Salcedo *et al* [42], in their study with mahogany seeds; reported that LEV did not form at the base of the wing. In this study, peak-dimple structures created by topography optimization reduced the flow velocity on the lower surface of the wing, while supporting the Leading Edge Vortex (LEV) formations on the upper part. Thus, an increase in the lift coefficient of the wing was achieved. This developed LEV structure seems to affect only the lift force in terms of aerodynamic performance. Although there is a minor reduction in the drag force due to friction, this reduction is not significant. As a result, considering all these effects, the fact that the LEV structure in biomimetic wings is an improvable phenomenon has been a remarkable point for future studies.

The fact that the results of the experimental studies with the M5 wing agree with the numerical study with the same wing shows the reliability of the numerical study used in the topography optimization. In addition, the experimental results of the M5 model have provided us with comparable consistent results on the aerodynamic performance of this biomimetic wing.

In the model M5, the highest C_L/C_D ratio was observed at 8° angle of attack at varying free stream velocities. This value varies between 1.7 and 2.00 according to experimental results. The stall angle at which the lifting force starts to drop suddenly in this model was determined at angles of attack close to 44°.

Aerodynamic performance features such as the late stalling feature and the contribution of LEVs to lift force were seen in the M0 and M5 designs. Scaling the models or improvements to the design did not change these properties. In addition, in the experiments carried out at free stream velocities of 6, 10 and 12 m/s, corresponding to the range of 22000-44000 Re, it was observed that the aerodynamic performance of the models did not change much depending on the velocity and exhibited a stable regime. While the C_L/C_D ratios generally remained greater than 1 up to angles of attack of 30°-35°, in the M0 and M5 models, they followed a stable regime according to changing angles of attack. Since the topography study enhanced the aerodynamic performance without changing the aerodynamic characteristics, the targeted development work has been achieved and a feasible data has been obtained for future studies.

Abbreviations

b	Span length
c	Mean chord length
C_D	Drag coefficient
C_L	Lift coefficient
D	Drag force
L	Lift force
P_{dyn}	Dynamic pressure
S	Planform area of the wing
V_∞	Free flow velocity
α	Angle of attack
ρ	Air density

Acknowledgements

M. E. Caliskan, is supported by The Council of Higher Education (CoHE) of Turkey with 100/2000 PhD Scholarship and by The Scientific and Technological Research Council of Turkey (TÜBİTAK) with 2211/A PhD Scholarship. M. U. Sabırlı and E. Oruç are supported by The

Scientific and Technological Research Council of Turkey (TÜBİTAK) with TÜBİTAK 2244- scholarship (Project no:118C100). In addition, this study was supported by the Scientific Research Project unit of Bursa Uludağ University (BAP) with the project number FGA-2022-620 and by the The Scientific and Technological Research Council of Turkey (TÜBİTAK) with the project number 124M308.

Data availability statement

The data presented in this study are available on request from the corresponding author.

Declarations

Conflict of interest The authors declare no conflict of interest.

References

[1] Benyus J M 1997 *Biomimicry: Innovation Inspired by Nature*, New York

[2] Aziz M S and El sheriff A Y 2016 Biomimicry as an approach for bio-inspired structure with the aid of computation. *Alex. Eng. J.* 55: 707–714

[3] Jiakun H, Zhe H, Fangbao T and Gang C 2021 Review on bioinspired flight systems and bionic aerodynamics. *Chin. J. Aeronaut.* 34: 170–186

[4] Perdomo O and Wei F S 2017 On the flapping motion of a helicopter blade. *Appl. Math. Modelling* 46: 299–311

[5] Chitsaz N, Siddiqui K, Marian R and Chahl J 2021 Numerical and experimental analysis of three-dimensional microcorrugated wing in gliding flight. *ASME. J. Fluids Eng.* 144: 011205. https://doi.org/10.1115/1.4051649

[6] Pan Y, Guo S, Whidborne J and Huang X 2024 Aerodynamic performance of a flyable flapping wing rotor with dragonfly-like flexible wings. *Aerosp. Sci. Technol.* 148: 109090. https://doi.org/10.1016/j.ast.2024.109090

[7] Gibbs-Smith C H 1967 *Leonardo da Vinci's aeronautics* HM Stationery Office, London

[8] Barroso E S, Ribeiro L G and Maia M A *et al*. 2022 BIOS: an object-oriented framework for Surrogate-Based Optimization using bio-inspired algorithms. *Struct. Multidisc Optim.* 65: 203. https://doi.org/10.1007/s00158-022-03302-0

[9] Rathod U H, Saha U K and Kulkarni V 2024 Bioinspired fluid dynamic designs of vertical-axis turbines: state-of-the-art review and the way forward. *ASME. J. Fluids Eng.* 146: 090801. https://doi.org/10.1115/1.4064753

[10] Yang Y, Zhu Q X and Wang W *et al*. 2021 Structure bionic design method oriented to integration of biological advantages. *Struct. Multidisc. Optim.* 64: 1017–1039. https://doi.org/10.1007/s00158-02102912-4

[11] Agnarsson I, Dhinojwala A, Sahni V and Blackledge T A 2009 Spider silk as a novel high performance biomimetic muscle driven by humidity. *J. Exp. Biology* 212: 1990–1994

[12] Yu Y, Pu G, Jiang T and Jiang K 2020 A dragonfly wing inspired biomimetic aerodynamic thrust bearing for increased load capacity. *Int. J. Mech. Sciences* 176: 105550. https://doi.org/10.1016/j.ijmecsci.2020.105550

[13] Liu K, Song B, Xue D, Yang W, Chen A and Wang Z 2022 Numerical study of the aerodynamic effects of bio-inspired leading-edge serrations on a heaving wing at a low Reynolds number. *Aerosp. Sci. Technol.* 124: 107529. https://doi.org/10.1016/j.ast.2022.107529

[14] Bang K, Kim J, Lee S I and Choi H 2016 Hydrodynamic role of longitudinal dorsal ridges in a leatherback turtle swimming. *Sci. Rep.* 6: 34283

[15] Wu F, Han A, Xie D, Yue Y and Yang C 2022 Effect of the wavy leading edge to aerodynamic performance improvement in a nuclear steam turbine last stage blade ES. *Energy Environ.* 16: 47–58

[16] Van Nierop E A, Alben S and Brenner M P 2008 How bumps on whale flippers delay stall: an aerodynamic model. *Phys. Rev. Lett.* 100: 054502

[17] Montoya E E H, Mendoza E and Stamhuis E J 2023 Biomimetic design of turbine blades for ocean current power generation. *Biomimetics* 8: 118

[18] Chu Y J 2016 A new biomimicry marine current turbine: study of hydrodynamic performance and wake using software OpenFOAM. *J. Hydrodyn.* 28: 125–141

[19] Holden J R, Caley T M and Turner M G 2015 Maple seed performance as a wind turbine 53rd AIAA Aerospace Science Meeting, p. 1304

[20] Lv J, Yang W, Zhang H, Liao D, Ren Z and Chen Q 2021 A feasibility study to reduce infrasound emissions from existing wind turbine blades using a biomimetic technique. *Energies* 14: 4923

[21] Tangermann E, Ercolani G and Klein M 2022 Aerodynamic behavior of a biomimetic wing in soaring flight–a numerical study. *Flow Turbul. Comb.* 109: 1155–1173

[22] Li Y, Yonezawa K, Xu R and Liu H 2021 A biomimetic rotor-configuration design for optimal aerodynamic performance in quadrotor drone. *J. Bionic Eng.* 18: 824–839

[23] Carré A, Gasnier P, Roux É and Tabourot L 2022 Extending the operating limits and performances of centimetre-scale wind turbines through biomimicry. *Appl. Energy* 326: 119996

[24] Ulrich E R, Pines D J and Humbert J S 2010 From falling to flying: the path to powered flight of a robotic samara nano air vehicle. *Bioinspir. Biomim.* 5: 045009

[25] Caliskan M E, Kaya F, Sabırlı M U and Karagoz I 2023 Design of a biomimetic wing from maple samara and investigation of the aerodynamic performance. *Phys. Fluids* 35: 095104

[26] Ribeiro A F P, Awruch A M and Gomes H M 2012 An airfoil optimization technique for wind turbines. *Appl. Math. Modelling* 36: 4898–4907

[27] Chen J, Wang Q, Zhang S, Eecen P and Grasso F 2016 A new direct design method of wind turbine airfoils and wind tunnel experiment. *Appl. Math. Modelling* 40: 2002–2014

[28] Gomes P and Palacios R 2020 Aerodynamic-driven topology optimization of compliant airfoils. *Struct. Multidisc. Optim.* 62: 2117–2130. https://doi.org/10.1007/s00158-020-02600-9

[29] Gomes P and Palacios R 2022 Aerostructural topology optimization using high fidelity modeling. *Struct. Multidisc. Optim.* 65: 137. https://doi.org/10.1007/s00158-022-03234-9

[30] Høghøj L C, Conlan-Smith C and Sigmund O *et al*. 2023 Simultaneous shape and topology optimization of wings.

Struct. Multidisc. Optim. 66: 116. https://doi.org/10.1007/s00158-023-03569-x

[31] Kear M, Evans B, Ellis R and Rolland S 2016 Computational aerodynamic optimization of vertical axis wind turbine blades. *Appl. Math. Modelling* 40: 1038–1051

[32] Raul V and Leifsson L 2023 Multifidelity aerodynamic shape optimization for mitigating dynamic stall using Cokriging regression-based infill. *Struct. Multidisc. Optim.* 66: 237. https://doi.org/10.1007/s00158-023-03690-x

[33] Abolpour B, Hekmatkhah R and Shamsoddini R 2022 A novel approach for obtaining optimum shape design with the minimum drag coefficient. *Struct. Multidisc. Optim.* 65: 306. https://doi.org/10.1007/s00158-022-03415-6

[34] Bomphrey R J, Lawson N J, Taylor G K and Thomas A L 2006 Application of digital particle image velocimetry to insect aerodynamics: measurement of the leading-edge vortex and near wake of a Hawkmoth. *Exp. Fluids* 40: 546–554

[35] Wu J H and Sun M 2004 Unsteady aerodynamic forces of a flapping wing. *J. Exp. Biol.* 207: 1137–1150

[36] Srygley R B and Thomas A L R 2002 Unconventional lift-generating mechanisms in freeflying butterflies. *Nature* 420: 660–664

[37] Ellington C P, Van Den Berg C, Willmott A P and Thomas A L 1996 Leading-edge vortices in insect flight. *Nature* 384: 626–630

[38] Sane S P 2003 The aerodynamics of insect flight. *J. Exp. Biol.* 206: 4191–4208

[39] Zuberi U A, Shahzad A, Qadri M N M, Shams T A and Zhao F W 2024 Effect of gurney flap on the aerodynamic performance of a flapping foil: micro-aerial vehicle application. *ASME. J. Fluids Eng.* 146: 011202. https://doi.org/10.1115/1.4063261

[40] Asadzadeh H, Moosavi A and Etemadi A 2019 Numerical simulation of drag reduction in microgrooved substrates using Lattice-Boltzmann method. *ASME. J. Fluids Eng.* 141: 071111. https://doi.org/10.1115/1.4042888

[41] Lentink D, Dickson W B, Van Leeuwen J L and Dickinson M H 2009 Leading-edge vortices elevate lift of autorotating plant seeds. *Science* 324: 1438–1440

[42] Salcedo E, Trevino C, Vargas R O and Martínez-Suástegui L 2013 Stereoscopic particle image velocimetry measurements of the three-dimensional flow field of a descending autorotating Mahogany seed (Swietenia macrophylla). *J. Exp. Biol.* 216: 2017–2030